SCHWEIZ. MINERAL. PETROGR. MITT. 78, 225–242, 1998

# Fluid composition at the blueschist – eclogite transition in the model system $Na_2O$–MgO–$Al_2O_3$–$SiO_2$–$H_2O$–HCl

by *Craig E. Manning*[1]

**Abstract**

The transformation of mafic epidote-blueschists to eclogites in subduction zones liberates water-rich fluids. Solute activities and concentrations in these high-pressure fluids are here estimated for the first time by taking advantage of correlations between the density of $H_2O$ and selected thermodynamic properties of aqueous ions and speciation reactions. Model mineral-solution equilibrium relations were computed in the system $Na_2O$–MgO–$Al_2O_3$–$SiO_2$–$H_2O$–HCl at 400 to 600 °C and 10 to 20 kb, conditions which span the boundary between the epidote-blueschist and eclogite facies in mafic rocks. Stoichiometric activity-activity diagrams indicate that $Na^+$ concentrations should exceed $Mg^{+2}$ concentrations by at least a factor of about $10^3$ for diverse crustal lithologies. For a range of mafic bulk compositions and mineral solid solutions, fluids in equilibrium with omphacite + garnet + quartz near the blueschist boundary were found to have severely restricted values of $\frac{a_{Na^+}}{a_{H^+}}$ and $\frac{a_{Mg^{+2}}}{a^2_{H^+}}$. Calculated elemental abundances are $SiO_2$ ~ Na ($10^{-0.5}$ molal) > Al ($10^{-2}$ to $10^{-3}$ molal > Mg ($10^{-7}$ molal) for total Cl concentrations up to 1.0 molal. The pH is strongly basic. Thus, fluids evolved from mafic rocks during eclogite formation should be rich in Si and Na, and have significantly higher Al contents than more familiar crustal fluids.

*Keywords:* NMASH-system, blueschist, eclogite, aqueous species, $H_2O$ density, activity diagrams.

## 1. Introduction

About 2 to 3 wt% of water-rich fluid is liberated when mafic blueschists transform to eclogites in subduction zones (PEACOCK, 1993). Fluid inclusion and phase equilibrium evidence indicate that many eclogite terranes equilibrated with a water-rich fluid (e.g., HOLLAND, 1979; SELVERSTONE et al., 1992; PHILIPPOT, 1993; NADEAU et al., 1993; MASSONNE, 1995). Large gradients in fluid pressure, coupled with low rock strength at $P_{fluid}$ near $P_{total}$, suggest that this fluid migrates away from the site of its liberation toward lower pressure environments, either up-dip in the subduction zone, or into the overlying mantle wedge. The large variations in rock composition that may exist along the flow-path of such a fluid produce the potential for substantial mass transfer. Oxygen-isotopic evidence and the metasomatic deposits that are common in exhumed subduction complexes indicate that mass transfer may be substantial (e.g., BEBOUT and BARTON, 1993). Incorporation of slab-derived alkalis and light rare-earth elements in high P/T metamorphic terranes and arc magmas attest to the significance of this process on a larger scale.

Unlike metasomatic environments found at shallow levels of the earth's crust, comparatively little is known about the major dissolved constituents of these fluids. Fluid inclusions indicate that salinities may range widely (PHILIPPOT, 1993; GIARAMITA and SORENSEN, 1994), but the relative abundances of major elements are virtually unknown. Phase-equilibrium constraints provide independent predictions of fluid composition in hydrothermal environments by successfully reproducing observed element concentrations (e.g., BIRD and NORTON, 1981). However, these methods require knowledge of the thermodynamic properties of minerals, fluids, and aqueous species at the conditions of interest. While important advances have recently been made in predicting

[1] Dept. of Earth and Space Sciences, University of California, Los Angeles, CA, 90095-1567, USA. <manning@ess.ucla.edu>

standard-state thermodynamic data for high-pressure minerals (e.g., HOLLAND and POWELL, 1990; EVANS, 1990; MASSONNE, 1995), similar data are lacking for aqueous species.

In this paper, I show that the equilibrium constants for reactions among aqueous species and the Gibbs free energies of relevant aqueous ions correlate approximately linearly with the logarithm of the density of $H_2O$ at constant temperature. This observation provides a framework for making provisional predictions of cation activities and species concentrations in aqueous solutions in equilibrium with blueschist and eclogite mineral assemblages. This paper focuses on the mineral-solution phase relations at the blueschist-eclogite transition using the model chemical system $Na_2O$–MgO–$Al_2O_3$–$SiO_2$–$H_2O$–HCl (NMASH).

## 2. Aqueous species at high pressures

### 2.1. EXPERIMENTAL AND PREDICTED THERMODYNAMIC PROPERTIES

The modified Helgeson-Kirkham-Flowers equation of state (HKF EOS; TANGER and HELGESON, 1988; SHOCK and HELGESON, 1988; SHOCK et al., 1989) is widely used for the computation of standard state thermodynamic properties of aqueous species for geochemical applications. The HKF EOS utilizes correlations among species-dependent parameters derived from experimental studies on relatively few solutes, as well as the density and dielectric constant of $H_2O$, to predict the properties of a wide range of aqueous species. However, knowledge of the dielectric constant of $H_2O$ to requisite accuracy is limited to ≤ 5 kb. Alternative approaches for estimating thermodynamic properties of aqueous species involve isocoulombic extrapolations (MESMER and BAES, 1974; GU et al., 1994), the correspondence principle (COBBLE, 1953), and correlations with the density of $H_2O$ (MARSHALL and FRANCK, 1981; MARSHALL and MESMER, 1984). Of these, density correlations have been explored in greatest detail at high pressures. The approach is based on the observation that the logarithms of the equilibrium constants (K) for many dissociation reactions are linear functions of the logarithm of the density of water ($\rho_{H_2O}$) at constant temperature. For example, MARSHALL and FRANCK (1981) showed that log K for the ionization of water was linear in log $\rho_{H_2O}$ to 4 kb (Fig. 1A). Numerous other dissociation reactions display similar behavior (EUGSTER and BAUMGARTNER, 1987; MESMER et al., 1988; ANDERSON et al., 1991). MANNING (1994a) found that such correlations could be extended to pressures of at least 20 kb based on experimentally determined log K values for the solubility of quartz (Fig. 1B).

The relations shown in figure 1 suggest that at constant temperature

$$\log K = a + b \log \rho_{H_2O} \quad (1)$$

To describe variations in log K over a range of temperatures and pressures, the $a$ and $b$ terms can be expanded to

$$a = a_1 + a_2T^{-1} + a_3T^{-2} + a_4T^{-3} \quad (2)$$

$$b = b_1 + b_2T^{-1} + b_3T^{-2} \quad (3)$$

(e.g., MESMER et al., 1988). Table 1 gives parameters derived by various authors from experimental determinations of several dissociation reactions for use with equations 1 to 3.

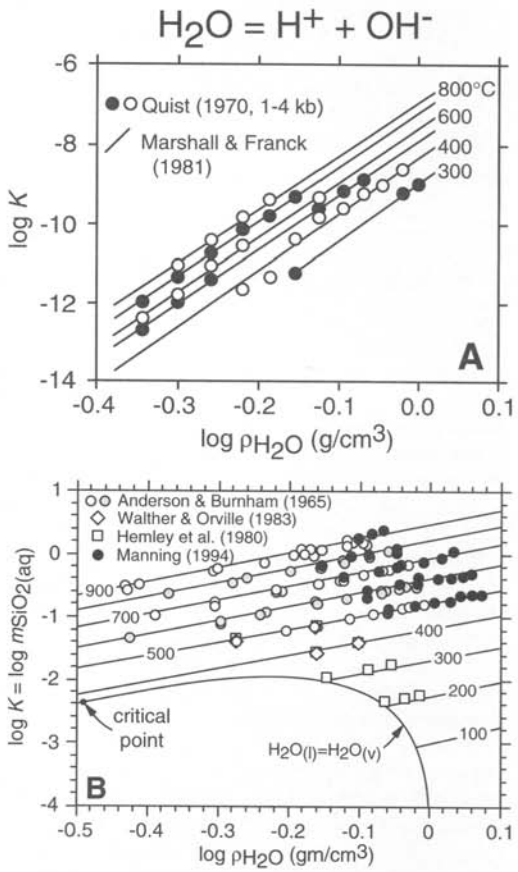


*Fig. 1* Logarithm of the density of water vs logarithm of the equilibrium constant for (A) the ionization of water, and (B) the solubility of quartz. Experimental data shown in symbols, polynomial fits (eq. 1 through 3) by solid lines.

*Tab. 1* Parameters for extrapolating experimentally determined log Ks (equations 1–3).

| | $a_1$ | $10^{-3}a_2$ | $10^{-5}a_3$ | $10^{-7}a_4$ | $10^{-1}b_1$ | $10^{-3}b_2$ | $10^{-5}b_3$ | ref. |
|---|---|---|---|---|---|---|---|---|
| $H_2O = H^+ + OH^-$ | –4.0980 | –3.2452 | 2.2362 | –3.9840 | 1.3957 | –1.2623 | 8.5641 | (1) |
| $HCl = H^+ + Cl^-$ | –5.4050 | 3.8749 | 0 | 0 | 1.3930 | 0 | 0 | (2) |
| $NaCl = Na^+ + Cl^-$ | –1.1970 | 1.2600 | 0 | 0 | 0.9200 | 0 | 0 | (3) |
| Quartz = $SiO_{2,aq}$ | 4.2620 | –5.7642 | 17.513 | –22.869 | 0.2845 | –1.0069 | 3.5689 | (4) |

References: (1) Marshall and Franck (1981); (2) Frantz and Marshall (1984); (3) Quist and Marshall (1968); (4) Manning (1994).

*Tab. 2* Parameters for extrapolating predicted log Ks using equation 1.

| | 400 °C | | 450 °C | | 500 °C | | 550 °C | | 600 °C | |
|---|---|---|---|---|---|---|---|---|---|---|
| | *a* | *b* | *a* | *b* | *a* | *b* | *a* | *b* | *a* | *b* |
| $NaOH = Na^+ + OH^-$ | 0.6964 | 8.5001 | 0.8371 | 8.9479 | 0.9829 | 9.1864 | 1.1356 | 9.4844 | 1.2848 | 9.7386 |
| $Mg^{+2} + H_2O = MgOH^+ + H^+$ | –5.4265 | –1.8848 | –5.0752 | –1.7838 | –4.7625 | –1.6350 | –4.4987 | –1.6645 | –4.2512 | –1.5805 |
| $Mg^{+2} + Cl^- = MgCl^+$ | 1.3397 | –8.6262 | 1.4776 | –9.0882 | 1.6149 | –9.3180 | 1.7469 | –9.5238 | 1.8819 | –9.6550 |
| $Al^{+3} + H_2O = AlOH^{+2} + H^+$ | –0.3937 | –7.7662 | –0.0207 | –6.5214 | 0.3423 | 5.3773 | 0.6156 | –5.1988 | 0.9293 | –4.5059 |
| $AlOH^{+2} = AlO^+ + H^+$ | –2.3800 | –3.4361 | –2.4068 | –3.2873 | –2.4672 | –3.2765 | –2.5328 | –3.1233 | –2.6062 | –2.9709 |
| $AlO^+ + H_2O = HAlO_2 + H^+$ | –2.1274 | 0.0024 | –2.1764 | –0.4251 | –2.2457 | –0.6387 | –2.3378 | –0.8587 | –2.4333 | –0.9612 |
| $HAlO_2 = AlO_2^- + H^+$ | –2.1703 | 7.0601 | –1.6651 | 7.4666 | –1.1843 | 7.7405 | –0.7252 | 7.9920 | –0.2837 | 8.2452 |

When combined with thermodynamic data of SHOCK et al. (1997) and SVERJENSKY et al. (1997), the revised HKF EOS (TANGER and HELGESON, 1988) also predicts isothermal linear dependence of log K on log $\rho_{H_2O}$. Figure 2 shows the variation in calculated log K with log $\rho_{H_2O}$ for the dissociation of NaOH and the first association of $Mg^{+2}$ with $OH^-$ and $Cl^-$. Values of log K are shown along the 400, 450, 500, 550 and 600 °C isotherms at log $\rho_{H_2O} > -0.2$ or $P > 2$ kb, at 0.5 kb intervals to 5 kb. The range 400 to 600 °C was selected because it is between these temperatures that the blueschist-eclogite transition occurs for many mafic bulk-rock compositions (EVANS, 1990; see below). Also shown for selected isotherms are estimated ± 0.5 kcal/mol average uncertainties in the predictions (e.g., SHOCK and HELGESON, 1988). The distribution of predicted log K values at 0.5 kb intervals at 2 to 5 kb is remarkably linear along isotherms. Similar results are obtained for Al hydrolysis reactions (Fig. 3). In detail the variations of log K with log $\rho_{H_2O}$ are nonlinear to varying degrees. This is illustrated in figure 3C, where log K for the reaction $AlO^+ + H_2O = HAlO_2 + H^+$ at 400 and 450 °C is plotted at a greatly expanded scale. However, comparison of the average uncertainties of the predicted log K values with the linear regression results in figures 2 and 3 demonstrates that fits to higher order polynomials are not justified by the data set.

The linear isothermal relationship between log K and standard molal Gibbs free energy (i.e., $\Delta G^\circ = -2.303\ RT \log K$) suggests that it would be fruitful to examine free energy changes with log $\rho_{H_2O}$ for individual ions. Figure 4 shows the variation in the conventional standard partial molal Gibbs free energy ($\Delta G^\circ$) of $Ca^{+2}$ with log $\rho_{H_2O}$, as calculated from equation of state parameters predicted by SHOCK and HELGESON (1988). At ≥ 500 °C, $\Delta G^\circ_{Ca^{+2}}$ increases with increasing $H_2O$ density to a maximum between 0.4 and 0.6 g cm$^{-3}$, depending on temperature. At higher densities, $\Delta G^\circ_{Ca^{+2}}$ decreases as $\rho_{H_2O}$ approaches 1.0 g cm$^{-3}$, which is the maximum density at which the HKF EOS is applicable. At ≤ 500 °C, $\Delta G^\circ_{Ca^{+2}}$ decreases with increasing density over the entire range of applicability of the HKF EOS. Inspection of the high density (high pressure) portions of each isotherm shows that their curvatures diminish as pressures increase, such that linear dependence of $\Delta G^\circ_{Ca^{+2}}$ on log $\rho_{H_2O}$ is approached at all temperatures. The pressure at which approximately linear behavior is exhibited increases from the liquid-vapor saturation pressure at ~ 200 °C to ~ 3.5 kb at 800 °C.

Predicted values of $\Delta G^\circ$ for $Na^+$, $Mg^{+2}$, and

$Al^{+3}$, the three bare-ion species relevant to the NMASH system, are shown as a function of log $\rho_{H_2O}$ in figure 5. The isothermal changes in $\Delta G^\circ$ appear to be very nearly linear in log $\rho_{H_2O}$. Fits to the equation

$$\Delta G_i^\circ = a + b \log \rho_{H_2O} \quad (4)$$

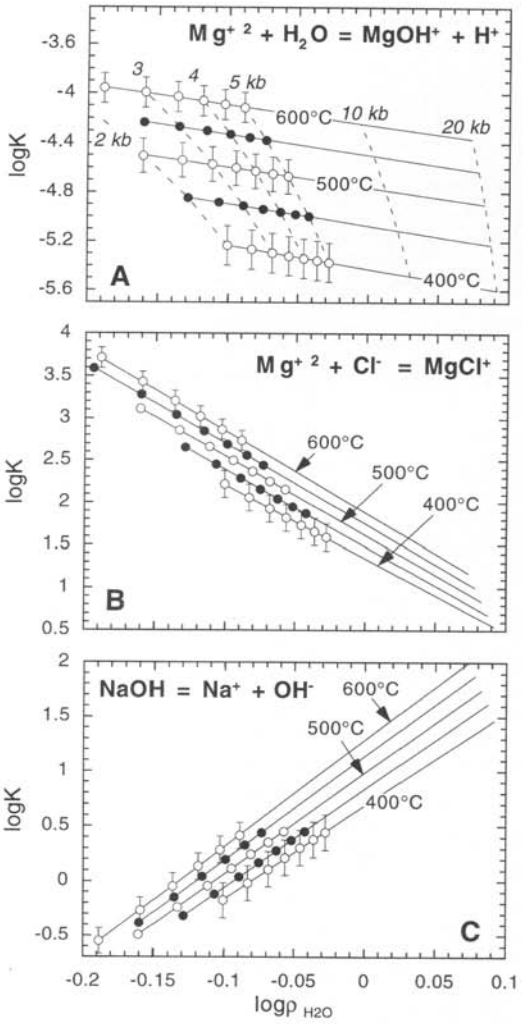


*Fig. 2* Values of log $\rho_{H_2O}$ vs log K for $Mg^{+2}$ (A and B) and $Na^+$ (C) reactions at 400 to 600 °C at 50 °C intervals. Predicted values (circles) are from SHOCK et al. (1997) and SVERJENSKY et al. (1997), and are plotted at 0.5 kb intervals from 2 or 2.5 to 5 kb, depending on the isotherm. Linear regression results (solid lines) extend beyond the predictions to $\rho_{H_2O}$ corresponding to 20 kb at each temperature. Resulting fit parameters given in table 2. Calculations employed SUPCRT92 (JOHNSON et al., 1992). Dashed curves in A are isobars.

at constant temperature yield the parameters given in table 3. The dependence of $\Delta G_i^\circ$ on density increases with increasing cationic charge (Fig. 5). Isothermal values of $\Delta G^\circ_{Na^+}$ depend only slightly on density, especially below 500 °C, whereas $\Delta G^\circ_{Al^{+3}}$ show a strong change with density at constant temperature. In addition, visual inspection shows that the greatest deviation from linear behavior is exhibited by $\Delta G^\circ_{Al^{+3}}$ at > 500 °C (Fig. 5C).

Generally high correlation correlation coefficients and visual inspection of departures from linearity in figures 2, 3 and 5 show that the density of water at high pressures provides a good guide for predicting how log K and $\Delta G_i^\circ$ changes with pressure, insofar as a large portion of their variance is explained by the independent variable. Moreover, given the average uncertainties in $\Delta G_i^\circ$, higher order polynomial fits are probably inappropriate, with the possible exception of $Al^{+3}$.

A potential explanation for the nearly linear behavior of log K and $\Delta G_i^\circ$ shown in figures 2 through 5 is the pressure-dependent changes in solvation and nonsolvation (electrostriction collapse) contributions to the properties of ions or reactions in the HKF model. At high pressures, nonsolvation contributions approach constant values, and the solvation contributions are simple functions of the density and dielectric constant of $H_2O$ (TANGER and HELGESON, 1988). As illustrated in figure 6, the isothermal variation in density and dielectric constant with pressure becomes markedly less nonlinear above ~ 3 kb. As a consequence, thermodynamic properties should be simple functions of density (or dielectric constant, or pressure) at high pressures. This is discussed in more detail by MANNING (1998a).

## 2.2. EXTRAPOLATIONS TO HIGH PRESSURES

While the HKF EOS is accurate over a P-T range that includes many upper to mid-crustal metamorphic environments, inaccuracies increase at $\rho_{H_2O} > 1.0$ g cm$^{-3}$ or P > 5 kb, precluding its use for metamorphic environments in which dense water is important. For example, figure 4 shows a schematic P-T path for subduction zone metamorphism in which the blueschist-eclogite transition is encountered at ~ 600 °C and 20 kb. Water densities exceed 1.0 g cm$^{-3}$ along the entire path.

The nearly linear isothermal variation of $\Delta G^\circ$ and log K with log $\rho_{H_2O}$ provides a framework for provisional extrapolation of these properties to high pressures. Figures 2, 3, and 5 show linear extrapolations of the fits from 5 to 20 kb. Although crude, there are four reasons that the extrapolations are reasonable estimates of high pressure

thermodynamic properties in the absence of further information. First, where experimental data exist, linear behavior of log K in log $\rho_{H_2O}$ is observed over this P-T range. In addition, as illustrated in figure 4, the extrapolation distance in log $\rho_{H_2O}$ coordinates is not extreme. The difference in log $\rho_{H_2O}$ between 2 and 5 kb is about the same as that between 5 and 20 kb, owing to the smaller increases in $\rho_{H_2O}$ with pressure at high pressure (Fig. 6). A third reason is that, as illustrated in figure 6, the variation in the density of water displays lower curvature at high pressures. Thus, neither discontinuities nor strong variations in first or second derivative properties are to be anticipated between 5 and 20 kb. Finally, the uncertainties in log K and $\Delta G^\circ$ shown in figures 2, 3, and 5 indicate that the additional degrees of freedom introduced by higher order, nonlinear fits are not justified at the levels of accuracy and precision of the predictions.

Provisional thermodynamic properties of aqueous ions and association/dissociation reactions derived through the linear extrapolations provide a framework for investigating a wide range of important mineral-solution equilibria. Applications to metamorphism along subduction zone and Barrovian metamorphic paths are discussed in more detail by MANNING (1998a). Below, I use the provisional data to explore phase relations and fluid composition in the model NMASH system at pressures and temperatures in the vicinity of the blueschist-eclogite transition.

## 3. Application to high-pressure solution-mineral equilibria

The transformation of mafic blueschist to eclogite is an important source of fluids in subduction zones. The migration of this fluid plays a critical role in driving retrograde hydration reactions at higher levels in the slab, and in causing metasomatic mass transfer in the overlying mantle wedge. What are the activity ratios of aqueous ions in fluids equilibrated with blueschist and eclogite facies minerals? How are they affected by mineral solid solutions? Most importantly, what are the compositions of the fluids released by

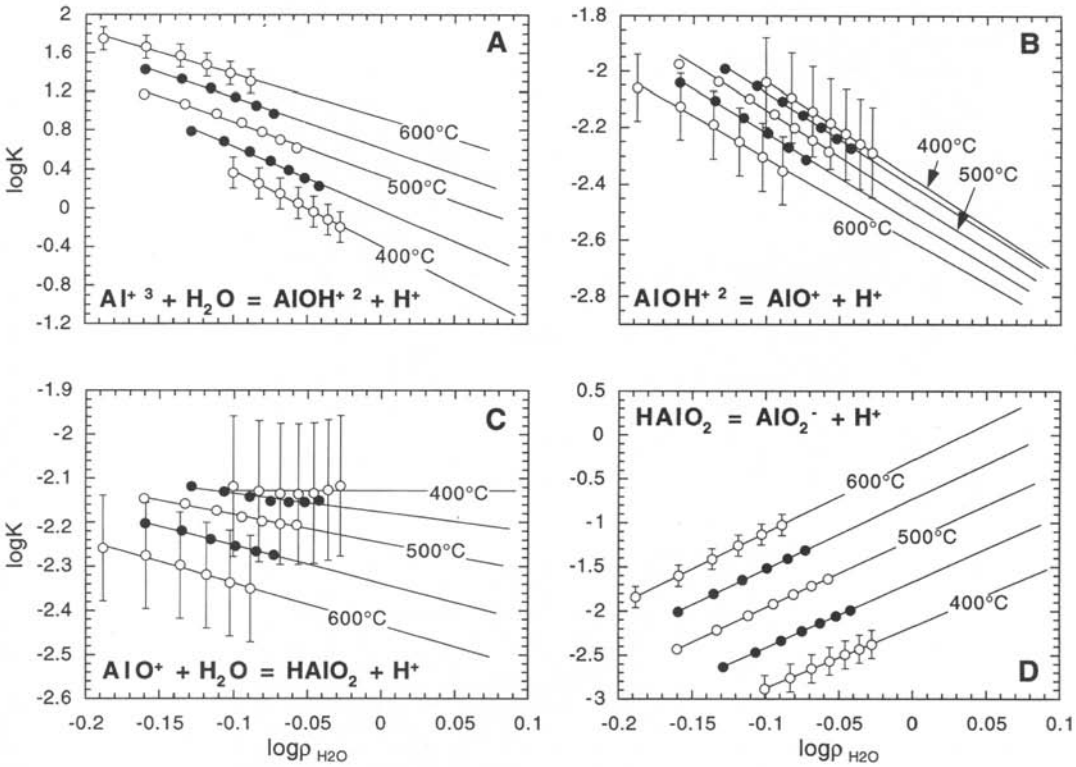


*Fig. 3* Values of log $\rho_{H_2O}$ vs log K for Al hydrolysis reactions at 400 to 600 °C. Predicted values (circles) are from SHOCK et al. (1997). See caption, figure 2.

blueschist dehydration? These questions are addressed by utilizing the extrapolated thermodynamic data derived in the first section of this paper.

All calculations employ thermodynamic data for minerals and $H_2O$ of HOLLAND and POWELL (1990) and the HAAR et al. (1984), respectively. HOLLAND and POWELL's (1990) data were used instead of BERMAN (1988) and EVANS (1990) because comparisons indicated little difference in calculated phase relations, and it was desirable to use the data set containing more mineral phase components (e.g., Mg-carpholite, Mg-staurolite, and amesite). Standard states for minerals and $H_2O$ are unit activities of pure phases at any pressure and temperature; for ions, the standard state was unit activity in the hypothetical 1 molal solution at any P and T, projected to infinite dilution.

### 3.1. EQUILIBRIUM ACTIVITY DIAGRAMS WITH STOICHIOMETRIC MINERALS

The best starting point for understanding mineral-solution equilibria is the construction of appropriate logarithmic activity-activity diagrams for stoichiometric minerals (e.g., GARRELS and CHRIST, 1965; HELGESON, 1970; BOWERS et al., 1984). Through such diagrams, the constraints imposed by rock-forming minerals on ion or electrolyte activities in the coexisting fluid can be evaluated. The hydrolysis of individual minerals such as talc can be written

$$\underset{\text{talc}}{Mg_3Si_4O_{10}(OH)_2} + 6\ H^+ = 3\ Mg^{+2} + 4\ SiO_{2,aq} + 4\ H_2O \qquad (5)$$

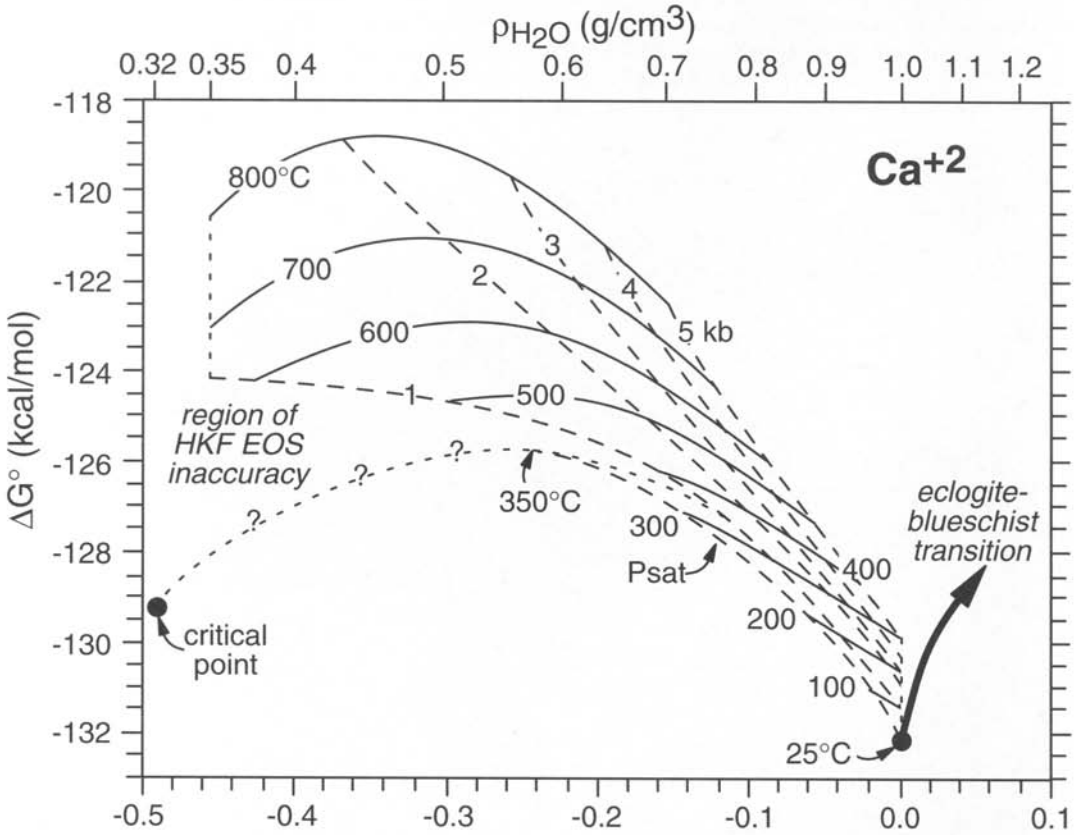


*Fig. 4* Convential standard partial molal Gibbs free energy of $Ca^{+2}$ vs log $\rho_{H_2O}$ from 25 to 800° and from $\rho_{H_2O}$ = 0.35 to 1.0 g cm$^{-3}$, based on the data of SHOCK and HELGESON (1988). Solid lines are isotherms; long dashed lines, isobars; short dashed lines delimit the region within which the Helgeson-Kirkham-Flowers equation of state (HKF EOS) allows calculation of thermodynamic properties to high accuracy. The arrow shows a subduction P-T path that would encounter the blueschist-eclogite transition; the HKF EOS is not suitable for calculation of $\Delta G°$ of aqueous ions for this metamorphic environment.

*Tab. 3* Parameters for extrapolating $\Delta G_i^\circ$ using equation (4).

| | 400 °C | | 450 °C | | 500 °C | | 550 °C | | 600 ° | |
|---|---|---|---|---|---|---|---|---|---|---|
| | *a* | *b* | *a* | *b* | *a* | *b* | *a* | *b* | *a* | *b* |
| $Na^+$ | –69.858 | 1.3984 | –71.229 | 1.6204 | –72.671 | –8.4118 | –74.137 | –1.3098 | –75.695 | –2.1026 |
| $Mg^{+2}$ | –100.44 | –28.693 | –99.567 | –27.995 | –98.649 | –26.714 | –97.690 | –25.446 | –97.137 | –28.031 |
| $Al^{+3}$ | –91.101 | –59.470 | –87.556 | –56.369 | –83.784 | –52.257 | –80.507 | –55.248 | –76.635 | –53.041 |

Units: kcal $mol^{-1}$

For pure talc and $a_{H_2O} = 1$, the mass action expression for reaction (5) leads to

$$\log \frac{a_{Mg^{+2}}}{a^2_{H^+}} = -\frac{4}{3}\log a_{SiO_2,aq} + \frac{1}{3}\log K_6 \qquad (6)$$

which is the equation for a line in $\log \frac{a_{Mg^{+2}}}{a^2_{H^+}}$ vs $\log a_{SiO_2,aq}$ coordinates. Given the standard molal Gibbs free energies of the pure phases (talc and $H_2O$) and the conventional standard partial molal Gibbs free energies of aqueous species (i.e., relative to $\Delta G^\circ_{H^+} = 0$), the equilibrium constant can be

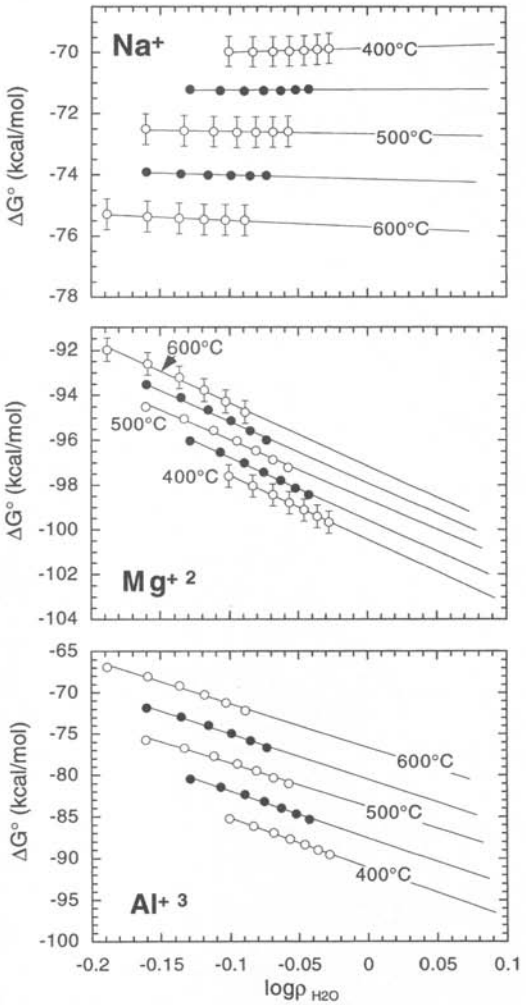


*Fig. 5* Values of $\log \rho_{H_2O}$ vs $\Delta G^\circ$ of $Na^+$, $Mg^{+2}$, and $Al^{+3}$ at 400 to 600 °C. Predicted values (circles) are from SHOCK and HELGESON (1988). See caption, figure 2.

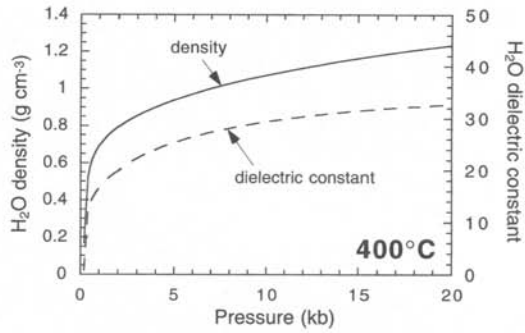


*Fig. 6* Comparison of the change in the density (HAAR et al., 1984) and dielectric constant (PITZER, 1983) of water with pressure at 400 °C.

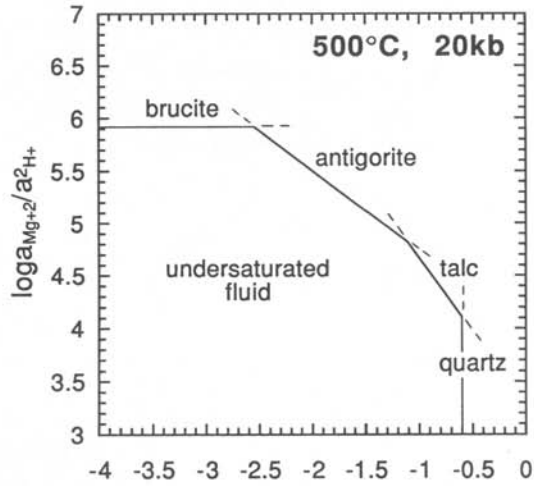


*Fig. 7* Equilibrium phase relations in the system MgO–$SiO_2$–$H_2O$–HCl as a function of $\log \frac{a_{Mg^{+2}}}{a^2_{H^+}}$ and $\log a_{SiO_2,aq}$ at 500 °C and 20 kb. Solid portions of lines represent stable phase boundaries; dashed lines are metastable.

calculated. Combining equation 6 with similar expressions for other minerals in the system $MgO–SiO_2–H_2O$ (MSH) thus allows computation of the values of log $\frac{a_{Mg^{+2}}}{a^2_{H^+}}$ and log $a_{SiO_2,aq}$ in equilibrium with all stable minerals.

Figure 7 shows equilibrium phase relations among minerals and an aqueous solution in the system $MgO–SiO_2–H_2O–HCl$ at 500 °C, 20 kb, in terms of log $\frac{a_{Mg^{+2}}}{a^2_{H^+}}$ and log $a_{SiO_2,aq}$. Solid parts of lines denote stable phase boundaries and dashed portions are metastable. Lines are isothermally-isobarically univariant; intersections represent isothermal-isobaric invariant points. Minerals stable with a fluid are those requiring the lowest val-

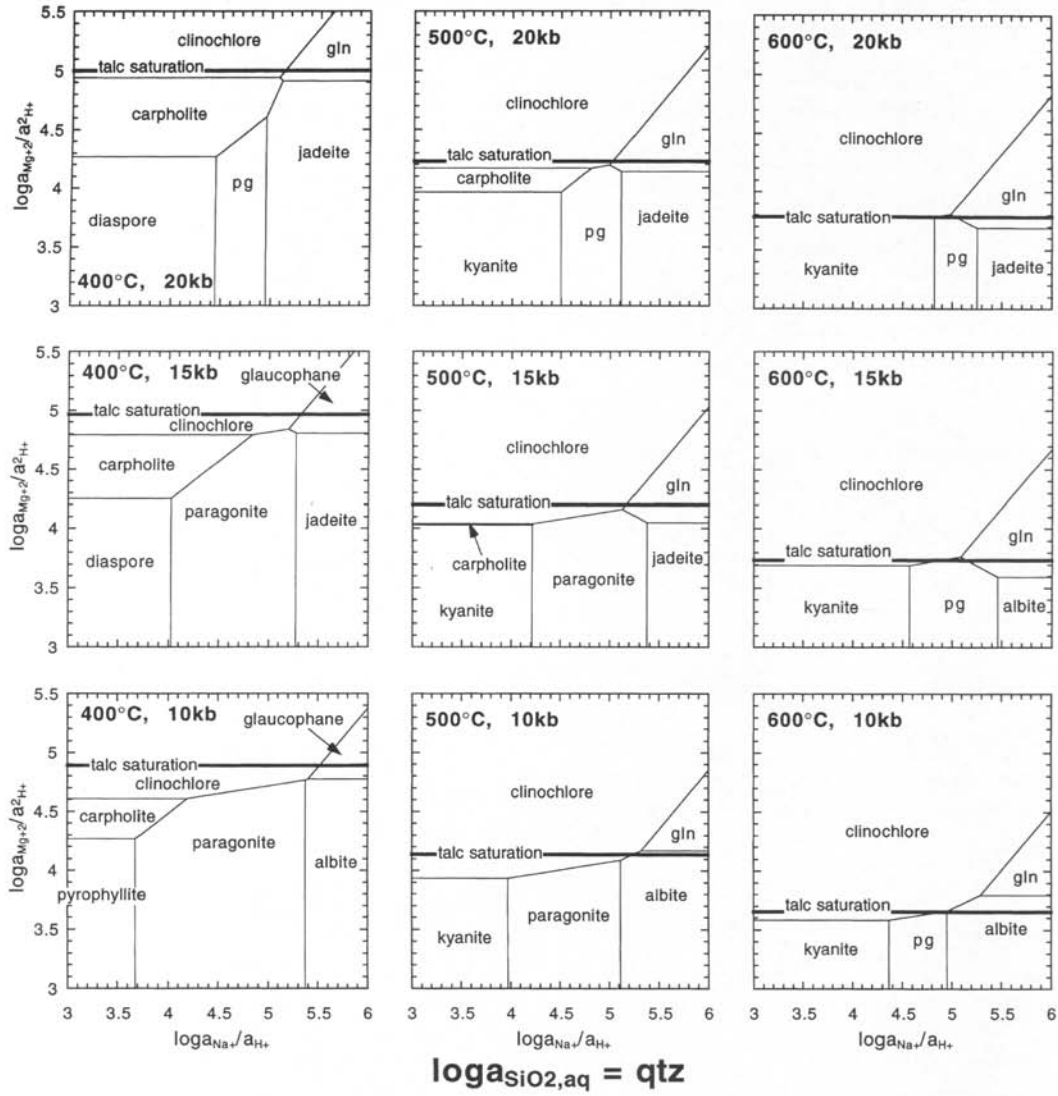


*Fig. 8* Equilibrium activity-activity diagrams showing phase relations among stoichiometric minerals in the NMASH system in the presence of quartz, in terms of log $\frac{a_{Mg^{+2}}}{a^2_{H^+}}$ and log $\frac{a_{Na^+}}{a_{H^+}}$. Diagrams drawn at constant pressure and temperature, from 400 to 600 °C, and from 10 to 20 kb. Thermodynamic data for minerals from HOLLAND and POWELL (1990). Mineral abbreviations after KRETZ (1983).

ue of $\frac{a_{Mg^{+2}}}{a^2_{H^+}}$ at a given $a_{SiO_2,aq}$ because of the correspondence between activity and chemical potential (e.g., HELGESON, 1970). A system composed solely of a very dilute fluid that is undersaturated with respect to all minerals is isothermally and isobariorcally divariant. Changes in activities (for example, by reaction with MSH minerals) cause the fluid to approach mineral saturation along any trajectory within the divariant field; for instance, by increasing $\frac{a_{Mg^{+2}}}{a^2_{H^+}}$ at constant pH and $a_{SiO_2,aq}$, by increasing $a_{SiO_2,aq}$ at constant $\frac{a_{Mg^{+2}}}{a^2_{H^+}}$, or by increasing both variables independently. When a mineral becomes saturated, the system is univariant because an additional phase has been added, so the system can only change at constant pressure and temperature by changing activities of $Mg^{+2}$, $H^+$, or $SiO_{2,aq}$. This may occur until a second solid phase saturates, at which point the composition of the fluid is isothermally-isobarically invariant. The only way to move off of the invariant point is to dissolve one of the two minerals. Fluid

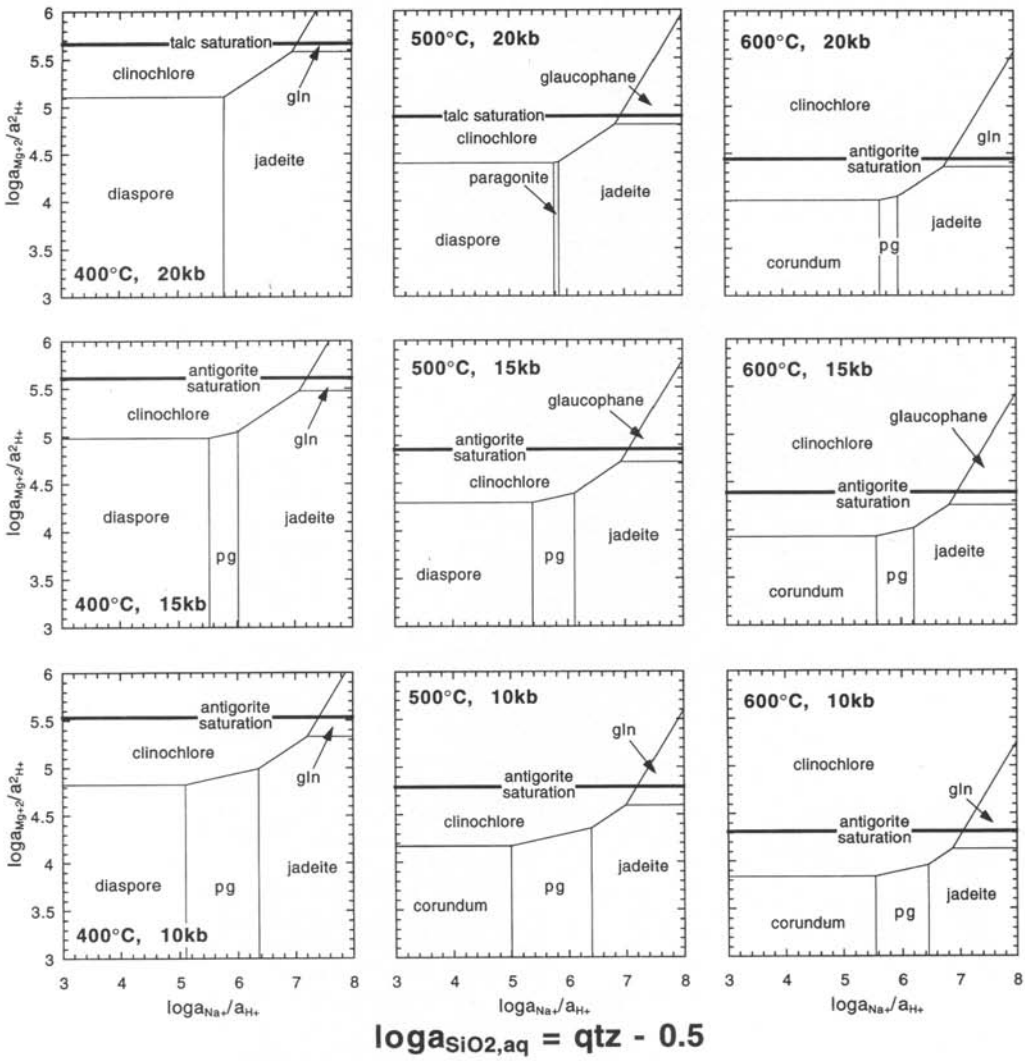


*Fig. 9* Equilibrium activity-activity diagrams showing phase relations among stoichiometric minerals in the NMASH system at log $a_{SiO_2,aq}$ equal to 0.5 units below quartz quartz saturation, in terms of log $\frac{a_{Mg^{+2}}}{a^2_{H^+}}$ and log $\frac{a_{Na^+}}{a_{H^+}}$. See caption, figure 8.

compositions plotting at higher activity ratios than the saturation surfaces are supersaturated, insofar as their activity ratios exceed those for equilibrium with the appropriate mineral; such fluids therefore do not reflect stable equilibrium, and the portions of the diagram beyond the saturation surfaces are not relevant to analysis of equilibrium phase relations. However, the relative plotting positions of supersaturated phases is often useful in unravelling metastable phase relations, such as the nucleation and growth of MSH phases during weathering of ultramafic rocks (e.g., NESBITT and BRICKER, 1978).

At 500 °C and 20 kb, MSH minerals stable with a fluid include brucite, antigorite, talc, and quartz (Fig. 7). The slopes of the saturation surfaces become less negative as log $a_{SiO_2,aq}$ decreases from a maximum at quartz saturation, through talc and antigorite, to brucite. These changes in slope reflect the changing Mg/Si in the solids. Similarly, the values of log $\frac{a_{Mg^{+2}}}{a^2_{H^+}}$ decrease from a maximum at brucite saturation. Note that at 500 °C and 20 kb, the only Mg-bearing phase stable with quartz is talc, and values below ~ 4 are insufficient to attain saturation with any Mg-bearing phase. Figure 7 illustrates that interaction between a silica-rich fluid liberated from a quartz-saturated rock and a hydrous ultramafic rock containing, for example, antigorite + brucite, would result in silica and Mg metasomatism. The consequences of the migration of silica-rich fluids in high pressure environments are discussed by MANNING (1995, 1996a).

Expanding the analysis of solution-mineral equilibria to more complex systems, such as the NMASH system, requires additional thermodynamic components, which in turn means that phase relations must be projected into two-dimensional coordinate systems for plotting purposes. This can be done by writing equilibria among NMASH phases such that Al is conserved in the minerals, and by fixing $a_{SiO_2,aq}$. For example, equilibrium between glaucophane and paragonite can be expressed as

$$3\ Na_2Mg_3Al_2Si_8O_{22}(OH)_2 + 22\ H^+ = \underset{\text{glaucophane}}{} \\ 2\ NaAl_3Si_3O_{10}(OH)_2 + 4\ Na^+ + 9\ Mg^{+2} + \underset{\text{paragonite}}{} \\ + 18\ SiO_{2,aq} + 12\ H_2O \qquad (7)$$

so

$$\log \frac{a_{Mg^{+2}}}{a^2_{H^+}} = -\tfrac{4}{9}\log \frac{a_{Na^+}}{a_{H^+}} + \\ + (\tfrac{1}{9}\log K_8 - 2\log a_{SiO_2,aq}) \qquad (8)$$

for stoichiometric minerals and pure $H_2O$. At constant pressure and temperature, silica activity is fixed in the presence of quartz (Fig. 7), so the terms in parentheses are constants, and equation 8 is the equation for a line in the coordinate system log $\frac{a_{Mg^{+2}}}{a^2_{H^+}}$ vs log $\frac{a_{Na^+}}{a_{H^+}}$. Alternatively, $a_{SiO_2,aq}$ can be fixed at another silica-buffering equilibrium (e.g., corundum-kyanite) or at an arbitrary value below quartz saturation. Diagrams constructed in this way display the same phase-rule variance relations as described for figure 7.

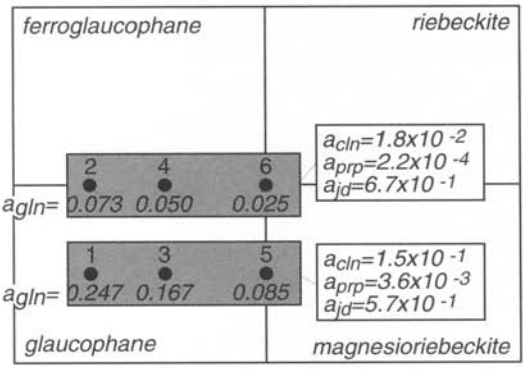


*Fig. 10* Sodic amphibole compositional space showing mineral compositions and activities used in the present study, after EVANS (1990). Activity of paragonite in white mica was 0.95 in all assemblages. Mineral abbreviations after KRETZ (1983), except: na-amp, sodic amphibole.

Figure 8 shows equilibrium phase relations among stoichiometric minerals in the NMASH system, at quartz saturation, 400, 500, and 600 °C, and 10, 15, and 20 kb. These P-T conditions were chosen to illustrate activity ratios near the blueschist to eclogite transition (EVANS, 1990). The diagrams simultaneously illustrate relevant mineral equilibria and information about fluid composition for different bulk compositions. Solid phases in the system $Al_2O_3$–$SiO_2$–$H_2O$ (ASH) that are stable with quartz include pyrophyllite, diaspore, and kyanite over the conditions considered; but neither pyrophyllite nor diaspore is stable with talc + quartz, whereas the assemblage talc + kyanite becomes stable at 600 °C between 15 and 20 kb. The relative stabilities of albite and jadeite in the presence of quartz illustrate the well-known pressure sensitivity over the P-T range considered. Pyrope is metastable over all conditions considered.

In addition to illustrating the familiar relations among solid phases, species activities required by minerals or assemblages of minerals are also given by the diagrams. For example, albite and jadeite reside at the highest log $\frac{a_{Na^+}}{a_{H^+}}$ and lowest log $\frac{a_{Mg^{+2}}}{a^2_{H^+}}$ at all conditions, and the activity ratios

in such limiting assemblages as paragonite-jadeite-quartz or glaucophane-jadeite-carpholite-quartz can be determined directly. Glaucophane stability is limited over the conditions considered, occupying a restricted compositional region at high $\log \frac{a_{Na^+}}{a_{H^+}}$ and $\log \frac{a_{Mg^{+2}}}{a^2_{H^+}}$ (Fig. 8). Predicted metastability with respect to albite + talc at low pressure and quartz saturation is consistent with experimental studies (KOONS, 1982; CARMEN and GILBERT, 1983; TROPPER et al., 1996, 1997). Carpholite stability expands with increasing pressure at 400 °C and 500 °C, and clinochlore stability is limited to the most Mg-rich and Na-poor bulk compositions. Both clinochlore and carpholite require that coexisting fluids have low $\log \frac{a_{Na^+}}{a_{H^+}}$.

Quartz-absent phase relations are displayed in figure 9. The degree of silica undersaturation required to form diaspore or corundum – minerals that are quite rare in blueschists and eclogites – is small in terms of $\log a_{SiO_2,aq}$, typically less than 0.5 log units (e.g, MANNING, 1996b). Phase relations at $\log a_{SiO_2,aq}$ equal to 0.5 units below quartz saturation should therefore correspond to the minimum silica activity in fluids in mafic rocks at high pressure. Figure 9 shows that diaspore and corundum are the stable ASH phases over the entire P-T range. Paragonite is less stable than at quartz saturation, as indicated by the more restricted range of $\log \frac{a_{Na^+}}{a_{H^+}}$ over which it occurs in figure 9 relative to figure 8. By contrast, the reduced silica activity causes jadeite and glaucophane to remain stable over the entire P-T range because of their lower silica contents relative to albite and talc. Carpholite, a comparatively silica-rich phase, is metastable with respect to clinochlore + corundum or diaspore at all conditions. Talc stability is much reduced relative to antigorite as compared with quartz saturation.

Figures 8 and 9 show that at each silica activity, maximum values of $\log \frac{a_{Mg^{+2}}}{a^2_{H^+}}$ (i.e., talc or antigorite saturation) decrease with isobaric increases temperature, and increase with isothermal increases in pressure. In addition, mineral assemblages involving a Mg-bearing phase require a fairly restricted range of $\log \frac{a_{Mg^{+2}}}{a^2_{H^+}}$ at 400–600 °C and 10–20 kb, regardless of silica activity. At quartz saturation (Fig. 8), values of $\log \frac{a_{Mg^{+2}}}{a^2_{H^+}}$ range from 3.6 (600 °C, 10 kb, clinochlore + kyanite) to 5.0 (400 °C, 20 kb, talc + clinochlore). At lower silica activity (Fig. 9), the minimum and maximum values occur at the same conditions, but are respectively 3.8 and 5.7, indicating that the possible range in $\log \frac{a_{Mg^{+2}}}{a^2_{H^+}}$ expands with decreasing silica activity. Such limits do not exist for $\log \frac{a_{Na^+}}{a_{H^+}}$ be cause there is no saturation surface analogous to talc; i.e., there is no rock-forming Al-free Na- or Na-Mg silicate. Thus, the minimum value of $\log \frac{a_{Na^+}}{a_{H^+}}$ constrained by the presence of a Na-bearing phase is 3.7 at 400 °C, 10 kb at quartz saturation (Fig. 8), and 5.0 at 500 °C, 10 kb at the lower silica activity (Fig. 9); but $\log \frac{a_{Na^+}}{a_{H^+}}$ can in theory attain quite large values.

Such limits are important because they provide a guide to the relative concentrations that might be anticipated in fluids in equilibrium with a range of mafic bulk compositions, which always contain Mg- and Na-bearing phases. Assuming fixed, neutral to basic pH values (see below) at 400–600 °C and 10–20 kb, the activity ratio limits imposed by the presence of Na- and Mg-bearing minerals in figures 8 and 9 translate $a_{Na^+}$ greater than $a_{Mg^{+2}}$ by a factor of more than $10^{3.5}$ at all conditions and all reasonable silica activities.

### 3.2. EQUILIBRIUM ACTIVITY DIAGRAMS AT THE BLUESCHIST-ECLOGITE TRANSITION WITH SOLID SOLUTIONS

The calculated phase relations described in the previous section can be applied to more realistic model bulk compositions by considering the effects of mineral solid solutions. EVANS (1990) presented an analysis of the phase relations at the epidote-blueschist to eclogite transition in the haplobasalt system (NCMASH), in which the facies boundary is defined by the model discontinuous reaction among phase components:

$$\underset{\text{glaucophane}}{13\ Na_2Mg_3Al_2Si_8O_{22}(OH)_2} + \underset{\text{clinozoisite}}{6\ Ca_2Al_3Si_3O_{12}(OH)} = \underset{\text{pyrope}}{9\ Mg_3Al_2Si_3O_{12}} + \underset{\text{jadeite}}{26\ NaAlSi_2O_6} + \underset{\text{diopside}}{12\ CaMgSi_2O_6} + \underset{\text{quartz}}{19\ SiO_2} + 16\ H_2O \qquad (9)$$

In mafic rocks, each phase component is an end member in a complex solid solution whose composition may vary with bulk composition, P, and T. EVANS (1990) explored the effects of different mineral compositions on the location of equilibrium 9; the compositions and phase component activities that he used are summarized in figure 10.

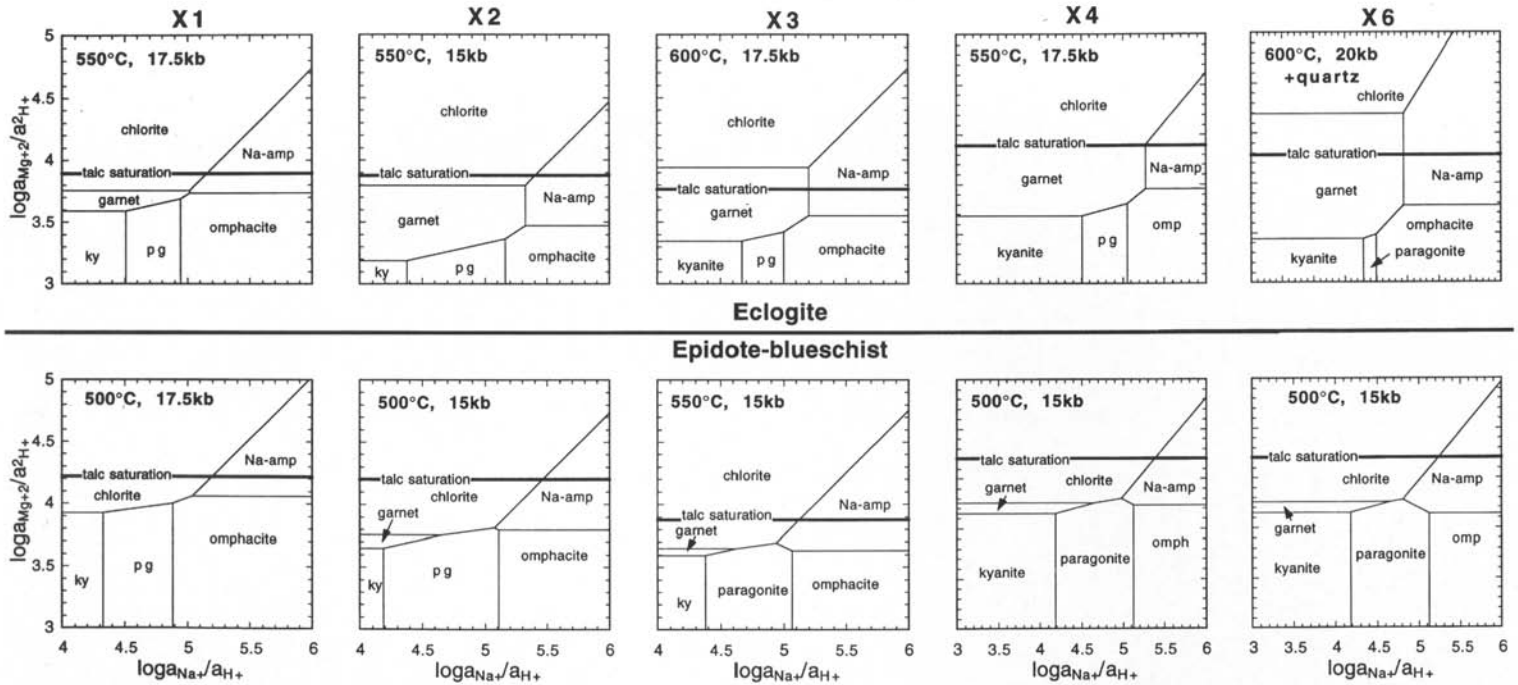


*Fig. 11* Equilibrium activity-activity diagrams showing phase relations among solid solutions in the NMASH system in the presence of quartz, in terms of $\log \frac{a_{Mg^{+2}}}{a^2_{H^+}}$ and $\log \frac{a_{Na^+}}{a_{H^+}}$. Diagrams give phase relations on either side of the blueschist-eclogite transition for bulk compositions X1–X4 and X6, which correspond to mineral compositions and activities given in figure 10. Mineral abbreviations after KRETZ (1983), except: cln, clinochlore.

He showed that equilibrium 9 has a steep, negative Clapeyron slope, and it occurs between ~ 500 to > 600 °C and 13 to > 20 kb for bulk compositions 1–6 (Fig. 10) at $a_{H_2O} = 0.9$.

The mineral compositions and activities of EVANS (1990) may be combined with projection of the phase relations into the Ca-free NMASH system to determine fluid activity ratios near the epidote-blueschist – eclogite transition. Reduced activities of phase components shift equilibrium phase boundaries in activity-activity diagrams through addition of nonzero terms to logarithmic mass-action expressions. For example, if glaucophane and paragonite are not end-member compositions, their activities are not unity, and equation 8 becomes

$$\log \frac{a_{Mg^{+2}}}{a^2_{H^+}} = -\tfrac{4}{9} \log \frac{a_{Na^+}}{a_{H^+}} + (\tfrac{1}{9} \log K_8 - 2 \log a_{SiO_2,aq} - \\ - 2 \log a_{paragonite} + 3 \log a_{glaucophane}) \qquad (10)$$

assuming pure $H_2O$. At quartz saturation and constant pressure and temperature, all the terms in the parentheses are constants, so equation 10 remains the expression for a straight line in $\log \frac{a_{Mg^{+2}}}{a^2_{H^+}}$ vs $\log \frac{a_{Na^+}}{a_{H^+}}$ coordinates. If the two mineral activity terms do not cancel, the intercept of the line described by equation 10 is shifted relative to equation 8, enlarging the stability field of the mineral for which the logarithmic activity term is greater in magnitude. Mineral-solution phase relations were calculated for all bulk compositions except X5, for which equilibrium (9) lies at > 600 °C below 20 kb; i.e., beyond the P-T range of the extrapolated thermodynamic data for aqueous species and association/dissociation reactions. Quartz was assumed to be present, and $a_{H_2O}$ was assumed to be 1.0 instead of 0.9 (cf., EVANS, 1990). For the purposes of comparison, the transition was assumed to be crossed either isobarically (X1 and X2) or by varying both P and T (X3, X4, and X6).

Activity diagrams illustrating mineral-fluid equilibria on either side of the transition from epidote-blueschist to eclogite (reaction 9) are shown in figure 11. The most important feature of the figure is that below the transition, the definitive eclogite assemblage of garnet + omphacite is not stable; instead, either garnet is unstable (X1), or assemblages involving sodic amphibole, paragonite, and chlorite intervene between omphacite and garnet. Once the transition is crossed, however, omphacite and garnet are stable together in all modeled bulk compositions. The stability of the assemblage omphacite + garnet is limited by sodic amphibole and paragonite; i.e., permitted true mafic eclogite assemblages in the presence of quartz include white mica + omphacite + garnet, omphacite + garnet, and amphibole + omphacite + garnet. The assemblage kyanite + omphacite + garnet is not predicted to be stable in the presence of quartz at the investigated pressure, temperature, and bulk composition; any combination of lower $a_{SiO_2}$, $a_{jadeite}$, $a_{pyrope}$, or higher $a_{paragonite}$, pressure, or temperature would result in kyanite-eclogite stability. Note that as glaucophane activity in sodic amphibole decreases from X1 through X6, its stability field expands (Fig. 11).

The transformation of epidote-blueschist to eclogite liberates a fluid phase (eq. 9), and the activity diagrams in figure 11 therefore constrain the equilibrium activity ratios in the fluid for the model NMASH system. Near the location of equilibrium (9), the assemblage omphacite + garnet + quartz must restrict activity ratios that are possible in the liberated fluids to a narrow range, regardless of bulk composition, pressure, or temperature (Fig. 11). The range of activity ratios must lie along the omphacite-garnet phase boundary between the omphacite-garnet-paragonite and omphacite-garnet-sodic amphibole invariant points. Values of $\log \frac{a_{Na^+}}{a_{H^+}}$ range from a minimum of 4.5 to a maximum of 5.3; corresponding $\log \frac{a_{Mg^{+2}}}{a^2_{H^+}}$ values are 3.4 to 4.0. This result implies that, independent of bulk composition or the precise pressure and temperature at which fluid is liberated during eclogite formation, the activity ratios of aqueous species near the blueschist-eclogite transition probably vary by no more than a factor of about ten.

### 3.3. FLUID COMPOSITION AT THE BLUESCHIST-ECLOGITE TRANSITION

Activity diagrams such as those in figures 8, 9, and 11 are useful for investigating the links between mineral assemblages, bulk composition, and the chemical potentials of components in the fluid phase. However, determining the concentrations of Na, Mg, Al, and Si in solution requires additional information. First, the important aqueous species of each of these elements must be identified, and thermodynamic data for their formation from the ionic species must then be derived. Tables 1–3 give the species considered in this study, and the parameters used for extrapolation of equilibrium constants to high pressures (Figs 2 and 3). $SiO_2$ is assumed to be a neutral monomer species because the pH values encountered in this study were not sufficiently high to allow for significant formation of $HSiO_3^-$; $NaHSiO_3$ and

$MgHSiO_3^+$ were ignored for similar reasons. Also, Al-chloride species were not considered, and the only complex of Na and Cl considered was NaCl (cf., OELKERS and HELGESON, 1990). Finally, possible Na-aluminate complexes (e.g., $NaAlO_2$) were ignored. Recent studies disagree over the stability of these complexes (POKROVSKII and HELGESON, 1995; ANDERSON, 1995); however, preliminary calculations and experiments (LIN and MANNING, 1997) suggest that even if such complexes are present, they are unlikely to represent a significant fraction of either Na or Al in high-pressure solutions.

The second requirement for translating calculated activity ratios to concentrations is an activity model for charged species. Although no experimental or theoretical study has specifically investigated the behavior of the Debye-Hückel activity model at high water densities, there is in principle no reason why it should not be applicable. Activity coefficients ($\gamma$) were therefore calculated using the Davies formulation (DAVIES, 1962):

$$\log \gamma_i = -\frac{Z_i^2 A\sqrt{I}}{1+\sqrt{I}} + 0.2\, A Z_i^2 \sqrt{I} \qquad (11)$$

where $Z_i$ is the charge of the $i$th species, $A$ is the species-independent Debye-Hückel parameter, and $I$ is the true ionic strength; i.e., the sum of the concentrations ($m$) of all species corrected for the formation of ion pairs and complexes:

$$I = \tfrac{1}{2}\sum_{i=1}^{n} m_i Z_i^2 \qquad (12)$$

The $A$ parameter varies strongly with pressure and temperature at low pressures, but it approaches constant values at $P > 4$ kb (HELGESON and KIRKHAM, 1974). Visual extrapolation of values predicted by HELGESON and KIRKHAM (1974) to 10 to 20 kb suggest that $A$ will be broadly within the range 0.7–1.2 $kg^{1/2}mol^{-1/2}$ at 400 to 600 °C. Sensitivity analyses indicated that speciation calculations show little dependence on the magnitude of $A$ within this range, so I used $A$ = 1.0 $kg^{1/2}mol^{-1/2}$ in the present study.

The Davies equation (eq. 11) is accurate to several percent at ionic strengths to 0.1 molal (DAVIES, 1962); at higher ionic strengths, accuracy is lower because the equation does not account for increasing ion association. Ionic strengths of eclogite-facies fluids calculated below are 0.1 to 1 molal, where the equation is probably accurate only to about ten per cent. Other activity coefficient equations account for ion association better, but they introduce additional unconstrained parameters. For this reason the Davies equation was viewed as the best path to a provisional estimate of eclogite-facies fluid compositions.

Using equations 11 and 12, the concentrations of relevant aqueous species in equilibrium with eclogite mineral assemblages can be determined. Fluid, quartz, omphacite, garnet, and either sodic amphibole or paragonite are compositionally invariant at constant pressure and temperature in the model NMASH system. Therefore $a_{SiO_2}$, $\frac{a_{Na^+}}{a_{H^+}}$, $\frac{a_{Mg^{+2}}}{a_{H^+}^2}$ and $\frac{a_{Al^{+3}}}{a_{H^+}^3}$ are fixed through the mass-action expressions for the hydrolysis of each of the four minerals (e.g., eq. 6). Solution for the fluid speciation and elemental concentrations involving $n$ aqueous species requires $n$–4 equations in addition to the four mass-action expressions, equation 12, and $n$ versions of equation 11. These are mass-action expressions for association/dissociation reactions (Tabs 1 and 2), and a charge balance equation or a concentration condition for Cl, if appropriate. Systems of $2n + 1$ nonlinear equations were solved using the program EQBRM (ANDERSON and CRERAR, 1993) for Cl-free and Cl-bearing aqueous solutions.

#### 3.3.1. Cl-free fluids

Species concentrations were calculated for pure $H_2O$ fluids for bulk compositions X1 to X4 and X6 (Fig. 12). Maximum and minimum concentrations are defined by the presence of paragonite or sodic amphibole; the widths of the rectangles in figure

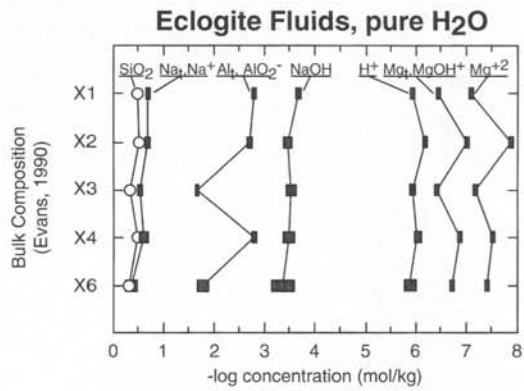


*Fig. 12* Individual species and total elemental concentrations for each of the bulk compositions investigated. Except for $SiO_2$, widths of rectangles correspond to the range in calculated concentrations for limiting assemblages of sodic amphibole eclogites and paragonite eclogites (see text). Pressures and temperatures of the calculations are those of the eclogite-facies activity-activity diagrams in figure 11.

12 denote the range in compositions permissible within these limiting assemblages. The calculated pH is ~ 6, regardless of bulk composition. Acid-base neutrality is ~ 3.5 at these conditions, so the calculated fluids are strongly basic. Total Si (as $SiO_{2,aq}$) and Na both have high concentrations of ~ 0.3 molal in Cl-free fluids in equilibrium with eclogite. Despite the basic pH, total Na ($Na_t$) is predominantly $Na^+$ because of the large log K for NaOH dissociation (Fig. 2). NaOH concentration is about three orders of magnitude below that of $Na^+$. The next highest elemental concentration is Al, which occurs as $AlO_2^-$ due to the high pH. Mg is very low in concentration and is predominantly present as $MgOH^+$, again as a consequence of the basic pH of the solution.

The model blueschist to eclogite transition occurs at progressively higher pressures and temperatures as bulk composition changes from X1 to X6 (EVANS, 1990). However, with the exception of Al, concentrations are only slightly dependent on these changes in P and T. For Al it can be seen that calculations performed at 600 °C (X3, X6) yield significantly higher total Al concentrations than at 550 °C.

### 3.3.2. Cl-bearing fluids

Chlorine is an important additional element likely to be present in fluids liberated at the blueschist to eclogite transition, and its variation in concentration will strongly influence speciation and elemental abundance in solution. Variations in fluid composition were calculated for total Cl ($Cl_t$) concentrations of 0.001 to 1.0 molal, or 0.006–6 weight percent NaCl equivalent. This range in chlorinities is appropriate for characterizing fluid-mineral equilibria involving dilute solutions, such as at the salinities of 1–5 weight percent NaCl (equivalent) found in fluid inclusions in mafic eclogites of the Franciscan Complex and the Catalina Schist, California, and the Samana Peninsula, Dominican Republic (GIARAMITA and SORENSEN, 1994). However, salinities of up to 14.5 weight percent NaCl equivalent are reported in the Monviso Complex of the Italian Alps (PHILIPPOT and SELVERSTONE,

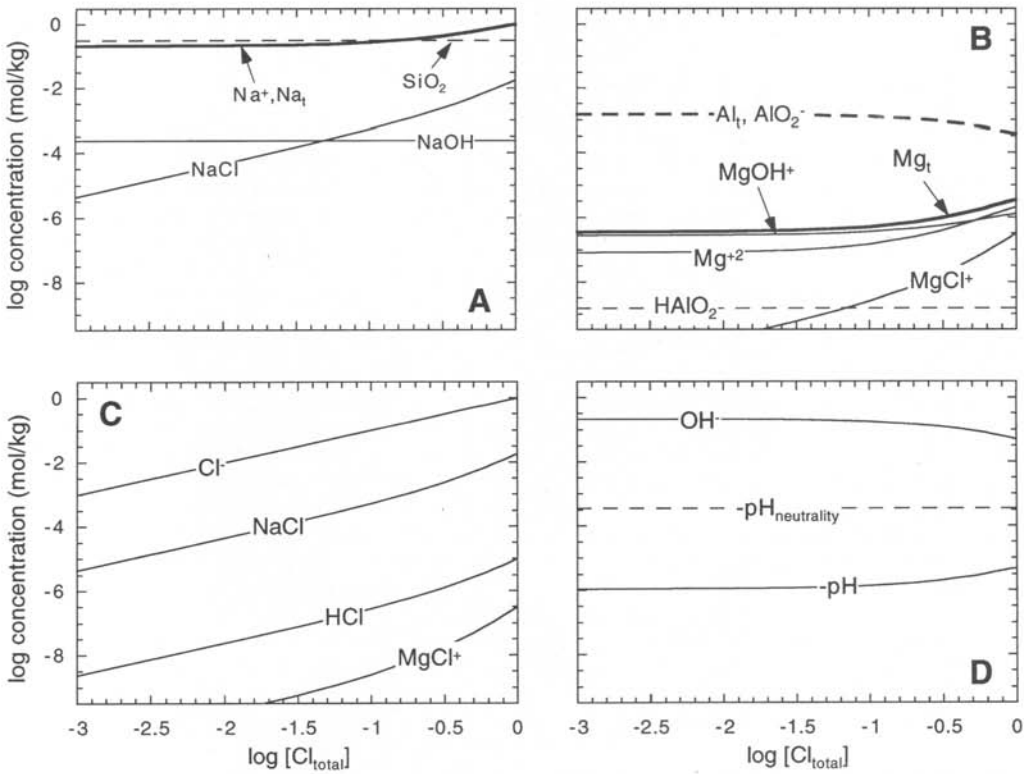


*Fig. 13* Individual species and total elemental concentrations vs total Cl concentration for X1 amphibole eclogite at 550 °C and 17.5 kb. Total elemental concentrations in bold lines, individual concentrations in light lines. In (D), ordinate is log concentration for $OH^-$, but log activity for pH.

1991); the calculations presented here are not applicable to such concentrated brines.

Figure 13A shows that $Na_t$ and $SiO_2$ remain high as $Cl_t$ concentration increases. The relative abundances cross over, such that $Na_t > SiO_2$, at ~ 0.2 molal $Cl_t$, as increasing NaCl abundance contributes to additional Na in solution. However, $Na^+$ remains the dominant sodium species throughout. Total Mg shows behavior similar to $Na_t$: $MgCl^+$ increases with $Cl_t$ and yields greater $Mg_t$ in solution (Fig. 13B). This effect is compounded by the increasing abundance of $Mg^{+2}$ due to decreasing pH (Fig. 13D). $MgOH^+$ is dominant until it is superceded by $Mg^{+2}$ at the highest Cl concentrations. In contrast, $Al_t$ decreases with increasing Cl. This is a combined effect of the decrease in the pH, which lowers the concentration of the dominant species $AlO_2^-$, and the absence of Al–Cl species from the calculations. Note that the extremely low stability of Al–Cl complexes at crustal conditions implies that, although not considered here, the calculated change in $Al_t$ concentration is probably real.

Figure 13C shows that, as should be expected, the abundance of all Cl-bearing aqueous species increases with increasing $Cl_t$. The dominant form of chlorine in solution is $Cl^-$ throughout the compositional range investigated. Increasing Cl concentrations registers an increase in pH only at > 0.1 molal (Fig. 13D) because the large value for $H_2O$ dissociation (–6.91) yields high concentrations of $OH^-$ in solution, so high concentrations of other anions are required before the charge balance will allow production of additional hydronium ions.

In summary, the calculated elemental abundances in aqueous fluid are $SiO_2$ ~ Na > Al > Mg from Cl concentrations of 0.001 to 1.0 molal; i.e., the order of element abundances do not show a strong dependence on Cl concentration over the range investigated. Also, pH is little affected by total Cl, decreasing by ~ 0.6 pH units but remaining strongly basic over the examined compositions. Although the accuracy of these calculations is limited by the applicability of equation 11 to these fluids, the relative concentrations of elements differ by orders of magnitude. The results of these calculations will likely not change significantly with improved computational methods.

## 4. Discussion and conclusions

Linear extrapolations of selected thermodynamic data for aqueous ions and speciation reactions provide the first opportunity to explore mineral-solution equilibria in high-pressure metamorphic environments. Stoichiometric activity-activity diagrams for the model NMASH system in the P-T range spanning the epidote-blueschist to eclogite transition (EVANS, 1990), indicate that $Na^+$ concentrations should be significantly greater than $Mg^{+2}$ concentrations for a broad range of lithologic types. After providing for mineral solid solutions reflecting a range of mafic bulk compositions, activity ratios in fluids are constrained by equilibrium with the eclogite assemblage omphacite + garnet + quartz near the blueschist boundary to a limited range in $\frac{a_{Na^+}}{a_{H^+}}$ and $\frac{a_{Mg^{+2}}}{a_{H^+}^2}$.

When the effects of ionic strength are taken into account, computed fluid compositions show several important features, which hold true regardless of the range of mineral compositions or aqueous Cl concentrations that were investigated. First, the calculated pH is basic (2–2.5 units above neutrality). This results from the combination of (1) the consumption of hydrogen ions as mineral hydrolysis reactions proceed (e.g., eq. 5), and (2) the predominance of positively charged ions in the dilute solutions explored in this study, which requires substantial concentrations of negatively charged species to maintain electrical neutrality. Because of the low abundance of $Cl^-$, $OH^-$ concentration must be significantly higher than that of $H^+$. Note that the large equilibrium constant for the ionization of $H_2O$ (Fig. 1A) dictates that the concentrations of both $H^+$ and $OH^-$ will be dramatically higher than in more familiar low pressure, low temperature environments.

Another important aspect of the calculated composition of fluids liberated by the production of mafic eclogites is that the elements with the greatest concentrations are Na and Si. High silica concentrations are to be expected because the rocks of interest are typically at or near quartz saturation, and quartz solubility in $H_2O$ is substantial at these conditions (MANNING, 1994, 1996b). The high silica contents and the large gradients in bulk composition associated with the juxtaposition of subducted crustal rocks against silica-poor ultramafic rocks of the mantle wedge generate the potential for substantial silica metasomatism; however, this metasomatism is likely to be localized to the slab-mantle interface because of the strong capacity of silica-poor rocks to consume this element through the production of progressively more silica-rich minerals (e.g., BEBOUT and BARTON, 1993; MANNING, 1995, 1996a). Sodium is somewhat less compatible than Si (e.g., PEARCE and PEATE, 1995), so the predicted high concentrations provide a means for mobilizing Na over larger length scales in the subduction zone–mantle wedge environment. However, the formation

of Na-silicates, such as sodic amphibole, may consume sufficient Na that its concentration is rapidly lowered as fluids migrate from their site of liberation. This appears to be the case in the mantle wedge above the Marianas back-arc region (STOLPER and NEWMAN, 1994).

A surprising result of the calculations of eclogite-facies fluid compositions is the elevated Al concentrations. These are in part a consequence of the enhanced solubility of Al because of the predominance of $AlO_2^-$, which means that Al contents increase as pH rises above the pK for the formation of this species from $HAlO_2$ in basic fluids. But independent experimental results also predict high Al solubilities in pure, nearly neutral $H_2O$. MANNING (1994b, 1998b) found that Al concentrations at 700 °C and 10 kb were ~$10^{-2}$ molal in equilibrium with kyanite and corundum. The experimental and theoretical results together suggest that the common observation of quartz and an aluminous phase such as kyanite in segregations and veins formed at eclogite-facies conditions (e.g., HEINRICH, 1982) require no special conditions or unusual ligands (cf., KERRICK, 1988); rather, they should be expected as a natural consequence of the strong increase of Al solubility with pressure.

Finally, the Mg concentration is calculated to be extremely low. This is a consequence of the low stability of the predominant complex, $MgOH^+$, at the basic pH values dictated by equilibrium between the dilute solutions and the eclogite-facies minerals. If this result is true for other divalent cations as well, then the calculations imply that low concentrations of Ca and Fe should be anticipated as well.

### Acknowledgements

I thank G. Anderson for kindly providing a copy of the program EQBRM. I thank J. Connolly and B. Evans for helpful reviews. Comments by D. Bird, R. Newton, and S. Sorensen also improved the manuscript. This work has benefitted from discussions with H. Lin and P. Tropper. Supported by NSF EAR-9405999.

### References

ANDERSON, G.M. (1995): Is there alkali-aluminum complexing at high temperatures and pressures? Geochim. Cosmochim. Acta, 59, 2155–2161.

ANDERSON, G.M. and BURNHAM, C.W. (1965): The solubility of quartz in supercritical water. Amer. J. Sci., 263, 494–511.

ANDERSON, G.M. and CRERAR, D.A. (1993): Thermodynamics in Geochemistry: The Equilibrium Model. New York, Oxford University Press, 588 pp.

ANDERSON, G.M., CASTET, S., SCHOTT, J. and MESMER, R.E. (1991): The density model for estimation of thermodynamic parameters of reactions at high temperatures and pressures. Geochim. Cosmochim. Acta, 55, 1769–1779.

BEBOUT, G.E. and BARTON, M.D. (1993): Metasomatism during subduction: products and possible paths in the Catalina schist. Chem. Geol., 108, 61–92.

BERMAN, R.G. (1988): Internally consistent thermodynamic data for minerals in the system $Na_2O$–$K_2O$–CaO–MgO–FeO–$Fe_2O_3$–$Al_2O_3$–$SiO_2$–$TiO_2$–$H_2O$–$CO_2$. J. Petrol., 29, 445–522.

BIRD, D.K. and NORTON, D. (1981): Theoretical prediction of phase relations among aqueous solutions and minerals: Salton Sea geothermal system. Geochim. Cosmochim. Acta, 45, 1479–1493.

CARMAN, J.H. and GILBERT, M.C. (1983): Experimental studies on glaucophance stability. Amer. J. Sci., 283-A, 414–437.

COBBLE, J.W. (1954): Empirical considerations of entropy. I. The entropies of oxy-anions and related species. J. Chem. Phys., 21, 1443–1456.

DAVIES, C.W. (1962): Ion Association, Butterworths, Washington D.C., 190 pp.

EUGSTER, H.P. and BAUMGARTNER, L. (1987): Mineral solubilities and speciation in supercritical metamorphic fluids. In: CARMICHAEL, I.S.E. and EUGSTER, H.P (eds): Thermodynamic modeling of geologic materials: minerals, fluids and melts. Rev. Mineralogy, 17, 367–403.

EVANS, B.W. (1990): Phase relations of epidote blueschists. Lithos, 25, 3–23.

FRANTZ, J.D. and MARSHALL, W.L. (1984): Electrical conductances and ionization constants of salts, acids, and bases in supercritical aqueous fluids. I: Hydrochloric acid from 100 to 700 °C and at pressures to 4000 bars. Amer. J. Sci., 284, 651–667.

GARRELS, R.M. and CHRIST, C.L. (1965): Solutions, Minerals, and Equilibria. Freeman, San Francisco, 450 pp.

GIARAMITA, M.J. and SORENSEN, S.S. (1994): Primary fluids in low-temperature eclogites: evidence from two subduction complexes (Dominican Republic, and California, USA). Contrib. Mineral. Petrol., 117, 279–292.

GU, Y., GAMMONS, C.H. and BLOOM, M.S. (1994): A one-term extrapolation method for estimating equilibrium constants of aqueous reactions at elevated temperatures. Geochim. Cosmochim. Acta, 58, 3545–3560.

HAAR, L., GALLAGHER, J.S. and KELL, G.S. (1984): NBS/ NRC Steam Tables. Hemisphere, New York, 320 pp.

HEINRICH, C.A. (1982): Kyanite-eclogite to amphibolite facies evolution of hydrous mafic and pelitic rocks, Adula Nappe, Central Alps. Contrib. Mineral. Petrol., 81, 30–38.

HELGESON, H.C. (1970): Description and interpretation of phase relations in geochemical processes involving aqueous solutions. Amer. J. Sci., 268, 415–438.

HELGESON, H.C. and KIRKHAM, D.H. (1974): Theoretical prediction of the thermodynamic behavior of aqueous electrolytes at high pressures and temperatures: II. Debye-Hückel parameters for activity coefficients and relative partial molal properties. Amer. J. Sci., 274, 1199–1261.

HEMLEY, J.J., MONTOYA, J.W., MARINENKO, J.W. and LUCE, R.W. (1980): Equilibria in the system $Al_2O_3$–$SiO_2$–$H_2O$ and some general implications for alteration/mineralization processes. Econ. Geol., 75, 210–228.

HOLLAND, T.J.B. (1979): Experimental determination of the reaction paragonite = jadeite + kyanite + $H_2O$, and internally consistent thermodynamic data for part of the system $Na_2O$–$Al_2O_3$–$SiO_2$–$H_2O$, with applications to eclogites and blueschists. Contrib. Mineral. Petrol., 68, 293–301.

HOLLAND, T.J.B. and POWELL, R. (1990): An enlarged and updated internally consistent thermodynamic dataset with uncertainties and correlations: the system $K_2O$–$Na_2O$–CaO–MgO–MnO–FeO–$Fe_2O_3$–$Al_2O_3$–$TiO_2$–$SiO_2$–C–$H_2O$–$O_2$. J. Metamorphic Geol., 8, 89–124.

JOHNSON, J.W., OELKERS, E.H. and HELGESON, H.C. (1992): SUPCRT92: A software package for calculating the stan-

dard molal thermodynamic perperties of minerals, gases, aqueous species, and reactions from 1 to 5000 bar and 0 to 1000 °C. Comp. Geosci., 18, 899–947.

KERRICK, D.M. (1988): $Al_2SiO_5$-bearing segregations in the Leopontine Alps, Switzerland: aluminum mobility in metapelites. Geology, 16, 636–640.

KOONS, P.O. (1982): An experimental investigation of the behavior of amphibole in the system $Na_2O$–MgO–$Al_2O_3$–$SiO_2$–$H_2O$ at high pressures. Contrib. Mineral. Petrol., 79, 258–267.

KRETZ, R. (1983): Symbols for rock-forming minerals. Amer. Mineral., 68, 277–279.

LIN, H. and MANNING, C.E. (1997): The solubility of albite-paragonite-quartz at 5 kbar, 350 °C. Geol. Soc. Amer. Abstr. Prog., 29/6, A-400.

MANNING, C.E. (1994a): The solubility of quartz in $H_2O$ in the lower crust and upper mantle. Geochim. Cosmochim. Acta, 58, 4831–4839.

MANNING, C.E. (1994b): Experimental determination of the solubilities of quartz, kyanite, and corundum in $H_2O$ in the lower crust and upper mantle. Min. Mag., 58A, 555–556.

MANNING, C.E. (1995): Phase-equilibrium controls on $SiO_2$ metasomatism by aqueous fluids in subduction zones: reaction at constant pressure and temperature. Int. Geol. Rev., 37, 1074–1093.

MANNING, C.E. (1996a): Coupled reaction and flow in subduction zones: silica metasomatism in the mantle wedge. In: JAMTVEIT, B. and YARDLEY, B.W.D. (eds): Fluid Flow and Transport in Rocks, London, Chapman & Hall, 139–148.

MANNING, C.E. (1996b): Effect of sediment on aqueous silica transport in subduction zones, In: BEBOUT, G.E., SCHOLL, D.W., KIRBY, S.H. and PLATT, J.P. (eds): Subduction Top to Bottom, Amer. Geophys. Union Mon. 96, 277–284.

MANNING, C.E. (1998a): Aqueous solutions at high pressure: I. Extrapolation schemes for estimating thermodynamic properties of aqueous ions at > 5 kb and high temperature. In preparation.

MANNING, C.E. (1998b): The solubility of kyanite + corundum in $H_2O$ at 700 °C, 1 GPa. In preparation.

MARSHALL, W.L. and FRANCK, E.U. (1981): Ion product of water substance, 0–1000 °C, 1–10'000 bars. New international formulation and its background. J. Phys. Chem. Ref. Data, 10, 295–304.

MARSHALL, W.L. and MESMER, R.E. (1984): Pressure-density relationships and ionization equilibria in aqueous solutions. J. Soln. Chem., 13, 383–391.

MASSONNE, H.-J. (1995): Experimental and petrogenetic study of UHPM. In: COLEMAN, R.G. and WANG, X. (eds): Ultrahigh Pressure Metamorphism. Cambridge University Press, Cambridge, 33–95.

MESMER, R.E. and BAES, C.F., Jr. (1974): Phosphoric acid dissociation equilibria in aqueous solutions to 300 °C. J. Soln. Chem., 3, 251–261.

MESMER, R.E., MARSHALL, W.L., PALMER, D.A., SIMONSON, J.M. and HOLMES, H.F. (1988): Thermodynamics of aqueous association and ionization reactions at high temperatures and pressures. J. Soln. Chem., 17, 699–718.

NADEAU, S., PHILIPPOT, P. and PINEAU, F. (1993): Fluid inclusion and mineral isotopic compositions (H–C–O) in eclogitic rocks as tracers of local fluid migration during high-pressure metamorphism. Earth Planet. Sci. Lett., 114, 431–448.

NESBITT, H.W. and BRICKER, O.P. (1978): Low temperature alteration processes affecting ultramafic bodies. Geochim. Cosmochim. Acta, 42, 403–409.

OELKERS, E.H. and HELGESON, H.C. (1990): Triple-ion anions and polynuclear complexing in supercritical electrolyte solutions. Geochim. Cosmochim. Acta, 54, 727–738.

PEACOCK, S.M. (1993): The importance of blueschist → eclogite dehydration reactions in subducting oceanic crust. Geol. Soc. Amer. Bull., 105, 684–694.

PEARCE, J.A. and PEATE, D.W. (1995): Tectonic implications of the composition of volcanic arc magmas. Ann. Rev. Earth Planet. Sci., 23, 251–285.

PHILIPPOT, P. (1993): Fluid-melt-rock interaction in mafic eclogites and coesite-bearing metasediments: constraints on volatile recycling during subduction. Chem. Geol., 108, 93–112.

PHILIPPOT, P. and SELVERSTONE, J. (1991): Trace-element-rich brines in eclogitic veins: implications for fluid composition and transport during subduction. Contrib. Mineral. Petrol., 106, 93–112.

PITZER, K.S. (1983): Dielectric constant of water at very high temperature and pressure. Proc. Natl. Acad. Sci. USA, 80, 4575–4576.

POKROVSKII, V.A. and HELGESON, H.C. (1995): Thermodynamic properties of aqueous species and the solubilities of minerals at high pressures and temperatures: the system $Al_2O_3$–$H_2O$–NaCl. Amer. J. Sci., 295, 1255–1342.

QUIST, A.S. (1970): The ionization constant of water to 800 °C and 400 bars. J. Phys. Chem. Ref. Data, 74, 3393–3402.

QUIST, A.S., and MARSHALL, W.L. (1968): Electrical conductances of aqueous sodium chloride solutions from 0 to 800 °C and at pressures to 4000 bars. J. Phys. Chem., 72, 684–703.

SELVERSTONE, J., FRANZ, G., THOMAS, S. and GETTY, S. (1992): Fluid variability in 2 GPa eclogites as an indicator of fluid behavior during subduction. Contrib. Mineral. Petrol., 112, 341–357.

SHOCK, E.L. and HELGESON, H.C. (1988): Calculation of the thermodynamic and transport properties of aqueous species at high pressures and temperatures: correlation algorithms for ionic species and equation of state predictions to 5 kb and 1000 °C. Geochim. Cosmochim. Acta, 52, 2009–2036.

SHOCK, E.L., HELGESON, H.C., and SVERJENSKY, D.A. (1989): Calculation of the thermodynamic and transport properties of aqueous species at high pressures and temperatures: Standard partial molal properties of inorganic neutral species. Geochim. Cosmochim. Acta, 53, 2157–2183.

SHOCK, E.L., SASSANI, D.C., WILLIS, M. and SVERJENSKY, D.A. (1997): Inorganic species in geologic fluids: correlations among standard molal thermodynamic properties of aqueous ions and hydroxide complexes. Geochim. Cosmochim. Acta, 61, 907–950.

STOLPER, E. and NEWMAN, S. (1994): The role of water in the petrogenesis of Mariana trough magmas. Earth Planet. Sci. Lett., 121, 293–325.

SVERJENSKY, D.A., SHOCK, E.L. and HELGESON, H.C. (1997): Prediction of the thermodynamic properties of aqueous metal complexes to 1000 °C and 5 kb. Geochim. Cosmochim. Acta, 61, 1359–1412.

TANGER, J.C. and HELGESON, H.C. (1988): Calculation of the thermodynamic and transport properties of aqueous species at high pressures and temperatures: revised equations of state for the standard partial molal properties of ions and electrolytes. Amer. J. Sci., 288, 19–98.

TROPPER, P., MANNING, C.E. and ESSENE, E.J. (1996): Experimental investigation of glaucophance stability in the system $Na_2O$–MgO–$Al_2O_3$–$SiO_2$–$H_2O$ (NMASH). Geol. Soc. Amer. Abstr. Prog., 28/7, A-158.

TROPPER, P., MANNING, C.E. and ESSENE, E.J. (1997): The composition of synthetic sodic high pressure amphiboles as a P-T indicator? An experimental approach and its consequences. Terra Nova Abstr. Suppl., 9/1, 38.

WALTHER, J.V. and ORVILLE, P.M. (1983): The extraction-quench technique for determination of the thermodynamic properties of solute complexes: application to quartz solubility in fluid mixtures. Amer. Mineral., 68, 731–741.

Manuscript received October 7, 1997; minor revision accepted March 3, 1998.